frontiers | Frontiers in Pharmacology

ORIGINAL RESEARCH
published: 22 July 2022
doi: 10.3389/fphar.2022.956154

A Pipeline for Natural Small Molecule Inhibitors of Endoplasmic Reticulum Stress

*Daniela Correia da Silva, Patrícia Valentão, Paula B. Andrade and David M. Pereira**

REQUIMTE/LAQV, Laboratório de Farmacognosia, Departamento de Química, Faculdade de Farmácia, Universidade do Porto, Porto, Portugal

The homeostasis of eukaryotic cells is inseverable of that of the endoplasmic reticulum (ER). The main function of this organelle is the synthesis and folding of a significant portion of cellular proteins, while it is also the major calcium reservoir of the cell. Upon unresolved ER stress, a set of stress response signaling pathways that are collectively labeled as the unfolded protein response (UPR) is activated. Prolonged or intense activation of this molecular machinery may be deleterious. It is known that compromised ER homeostasis, and consequent UPR activation, characterizes the pathogenesis of neurodegenerative diseases. In an effort to discover new small molecules capable of countering ER stress, we subjected a panel of over 100 natural molecules to a battery of assays designed to evaluate several hallmarks of ER stress. The protective potential of these compounds against ER stress was evaluated at the levels of calcium homeostasis, key gene and protein expression, and levels of protein aggregation in fibroblasts. The most promising compounds were subsequently tested in neuronal cells. This framework resulted in the identification of several bioactive molecules capable of countering ER stress and deleterious events associated to it. Delphinidin stands out as the most promising candidate against neurodegeneration. This compound significantly inhibited the expression of UPR biomarkers, and displayed a strong potential to inhibit protein aggregation in the two aforementioned cell models. Our results indicate that natural products may be a valuable resource in the development of an effective therapeutic strategy against ER stress-related diseases.

Keywords: endoplasmic reticulum stress, unfolded protein response, drug discovery, neurodegeneration, natural products

OPEN ACCESS

Edited by:
Kah Hui Wong,
University of Malaya, Malaysia

Reviewed by:
Hakim Manghwar,
Lushan Botanical Garden (CAS), China
Jun Ren,
University of Washington, United States

****Correspondence:***
David M. Pereira
dpereira@ff.up.pt

Specialty section:
This article was submitted to Ethnopharmacology, a section of the journal Frontiers in Pharmacology

Received: *29 May 2022*
Accepted: *21 June 2022*
Published: *22 July 2022*

Citation:
Correia da Silva D, Valentão P, Andrade PB and Pereira DM (2022) A Pipeline for Natural Small Molecule Inhibitors of Endoplasmic Reticulum Stress. Front. Pharmacol. 13:956154. doi: 10.3389/fphar.2022.956154

INTRODUCTION

The endoplasmic reticulum (ER) plays a substantial role in the upkeep of the proteostasis of any eukaryotic cell. Upon unresolved ER stress, several stress response signaling pathways are activated in this organelle. These pathways are collectively termed as the unfolded protein response (UPR) and aim to restore reticular homeostasis, but may be deleterious upon sustained or intense activation. Shortly, the UPR relies on three major signaling branches, each initiated by its respective sensor: the protein kinase RNA-like endoplasmic reticulum kinase (PERK), inositol-requiring enzyme 1 (IRE1) or the activating transcription factor 6 (ATF6) (Pereira et al., 2015; da Silva et al., 2020).

Disturbances in the secretory pathway of proteins and consequent stress upon the ER are hallmarks of several disease etiologies, including those of neurodegenerative nature. Presently,

neurodegenerative diseases have a high prevalence around the world, and their incidence is expected to increase as the population ages (Xiang et al., 2017; Taalab et al., 2018; da Silva et al., 2020). Pharmacological intervention by modulating ER stress has shown promising results against neurodegeneration *in vitro* and *in vivo* (O'Connor et al., 2008; Plate et al., 2016; Cissé et al., 2017; Duran-Aniotz et al., 2017). Accordingly, we consider the development of ER-based strategies against neurodegenerative diseases a necessary step to overcome the burden that these diseases represent to society.

Natural products have been used as medicinal agents from immemorial times and remain the best source of lead compounds and new drugs to modern medicine (Cragg and Newman, 2001). This chemical space has been gifted with immense structural diversity and has been evolutionarily tailored to provide drug-like molecules, displaying multiple chemotypes and pharmacophores (Cragg and Newman, 2001; Shen, 2015). Furthermore, it is known that the time when pharmaceutical companies decided to reduce natural product research projects correlates with decreased numbers of new drugs entering the market (Shen, 2015). A literature survey on nature-derived ER modulators (Pereira et al., 2015) shows the importance of the natural product chemical space for this end, including molecules as distinct as basiliolides (Navarrete et al., 2006), fisetin (Syed et al., 2014; Kang et al., 2016; Shih et al., 2017), berberine (Wang et al., 2010; Hao et al., 2012; Zhang et al., 2016), withaferin A (Choi et al., 2011; Khan et al., 2012), agelasine B (Pimentel et al., 2012), cephalostatin 1 (López-Antón et al., 2006; Tahtamouni et al., 2018), and hydroxytyrosol (Giordano et al., 2013). Notably, most of these molecules are associated to ER stress induction, while hydroxytyrosol and berberine are reported to ameliorate ER stress.

Herein we propose a pipeline for the identification of potential ER stress inhibitors among a library of natural products.

MATERIALS AND METHODS

Chemical Library and Reagents

The compounds 5,7,8-trihydroxyflavone, 5-deoxykaempferol, acacetin, apigenin, apigetrin, β-escin, chrysoeriol, chrysophanol, coumarin, cyanidin, delphinidin, diosmetin, diosmin, ellagic acid, eriocitrin, eriodictyol, eriodictyol-7-*O*-glucoside, eupatorin, ferulic acid, fisetin, flavanone, galangin, gallic acid, genkwanin, gentisic acid, guaiazulene, herniarin, hesperidin, homoeriodictyol, homoorientin, homovanillic acid, hyoscyamine, isorhamnetin, isorhamnetin-3-*O*-glucoside, isorhamnetin-3-*O*-rutinoside, isorhoifolin, juglone, kaempferide, kaempferol, kaempferol-3-*O*-rutinoside, kaempferol-7-*O*-glucoside, kaempferol-7-*O*-neohesperidoside, linarin, liquiritigenin, lutein, luteolin, luteolin tetramethylether, luteolin-3′,7-di-*O*-glucoside, luteolin-4′-*O*-glucoside, luteolin-7-*O*-glucoside, malvidin, mangiferin, maritimein, myricetin, myricitrin, myrtillin, naringenin-7-*O*-glucoside, narirutin, oleuropein, orientin, pelargonidin, pelargonin, phloroglucinol, pyrogallol, quercetin-3-*O*-(-6-acetylglucoside), quercetagetin, quercetin-3,3′,4′,7-tetramethylether, quercetin-3,4′-dimethylether, quercetin-3-methylether, quercetin-3-*O*-glucuronide, rhoifolin, robinin, saponarin, scopolamine, sennoside A, sennoside B, sulfuretin, tectochrysin, tiliroside, verbascoside and vitexin were purchased from Extrasynthese (Genay, France). The molecules (-)-norepinephrine, (+/-)-dihydrokaempferol, 1,4-naphtoquinone, 18α-glycyrrhetinic acid, 3,4-dihydroxybenzoic acid, 3,4-dimethoxycinnamic acid, 3-hydroxybenzoic acid, 4-hydroxybenzoic acid, 5-methoxypsoralen, ajmalicine, berberine, betanin, betulin, boldine, catechol, cholesta-3,5-diene, chrysin, cynarin, daidzein, emodin, galanthamine, genistein, guaiaverin, hesperetin, hydroquinone, lupeol, myristic acid, naringenin, naringin, *p*-coumaric acid, phloridzin, pinocembrin, plumbagin, quercetin, quercetin-3-*O*-β-D-glucoside, quercitrin, rosmarinic acid, rutin and silibinin were acquired from Sigma-Aldrich (St. Louis, MO, United States). 5,8-Dihydroxy-1,4-naphthoquinone and caffeine were from Fluka (Buchs, Switzerland), vanillin was supplied by Vaz Pereira (Santarém, Portugal), vicenin-2 was purchased from Honeywell (Charlotte, NC, United States). Chlorogenic acid was from PhytoLab (Vestenbergsgreuth, Germany). Cinnamic acid was obtained through Biopurify (Chengdug, China). Swertiamarin was from ChemFaces (Wuhan, China).

Minimum Essential Medium (MEM), Dulbecco's Modified Eagle Medium/Nutrient Mixture F-12 (DMEM/F-12), fetal bovine serum, penicillin/streptomycin solution (penicillin 5,000 units/mL and streptomycin 5,000 μg/ml), trypsin-EDTA (0.25%), Qubit® RNA IQ assay kit and Qubit® RNA HS assay kit, the SuperScriptTM IV VILOTM MasterMix, the Qubit® Protein Assay Kit, the anti-BiP mouse monoclonal antibody (Catalog # MA5-15619, lot WI3375321) and the anti-mouse secondary antibody (Catalog # 61-6,520, lot WB319554) were obtained from Invitrogen (Grand Island, NE, United States). Dimethyl sulfoxide (DMSO) was acquired from Fisher Chemical (Loughborough, United Kingdom). Isopropanol was obtained from Merck (Darmstadt, Germany). 3-(4,5-Dimethylthiazol-2-yl)-2,5-diphenyltetrazolium bromide (MTT), calcium ionophore A23187, thapsigargin, RNAzol®, chloroform, isopropanol, diethyl pyrocarbonate (DEPC), KAPA SYBR® FAST qPCR Kit Master Mix (2X) Universal, $A\beta_{25-35}$, 2-(4-amidinophenyl)-6-indolecarbamidine dihydrochloride (DAPI), protease inhibitor cocktail, phosphatase inhibitor cocktail, acrylamide/bis-acrylamide 30% solution, bromophenol blue, glycerol, sodium dodecylsulfate (SDS), glycine, Trizma® base, Trizma® hydrochloride, sodium deoxycholate, sodium chloride, potassium phosphate monobasic, potassium chloride, sodium phosphate dibasic, sodium bicarbonate, D-glucose and Triton X-100 were purchased from Sigma-Aldrich (St. Louis, MO, United States), while formaldehyde was from Bio-Optica (Milan, Italy). The fluorescent probe Fura-2/AM, as well as the anti-GAPDH (Catalog # ab181602) rabbit monoclonal antibody and the anti-rabbit secondary antibody (Catalog # ab6721, lot GR172025-6) were obtained from Abcam (Cambridge, United Kingdom). Thioflavin T was from Alfa Aesar (Kandel, Germany). The WesternBright® ECL HRP was supplied by Advansta (Menlo Park, CA, United States). Trans-Blot Turbo Mini 0.2 μm Nitrocellulose Transfer Packs were acquired from Bio-Rad (Hercules, CA, United States).

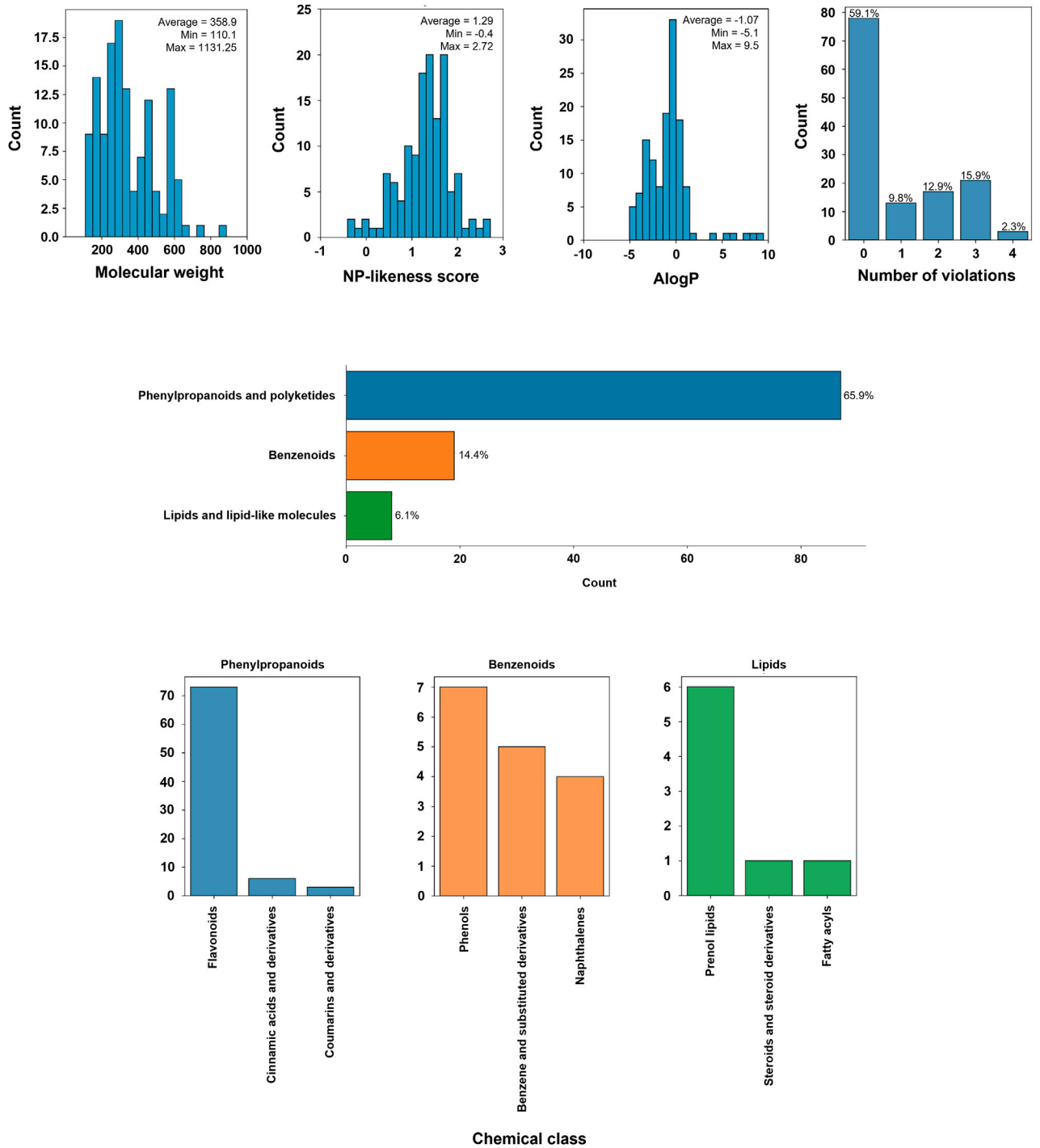

FIGURE 1 | Physico-chemical properties of the library used (molecular weight, NP-likeness score, AlogP, Number of Lipisnki violations), and distribution of the chemical (super)classes of the molecules present in the library.

Chemometric Analysis

Since it is the most detailed and up to date database of annotated natural products (Sorokina et al., 2021), we started from the COCONUT database (https://coconut.naturalproducts.net) and created a data frame comprising all the molecules under study, where each row corresponded to a different molecule and columns to features. Among all the original features, we have decided to keep only 48, as the remaining ones did not contain relevant information for this work (SMILE notation, fragments, among others). **Supplementary Table S3** contains a list of all

variables kept and their description. All data was cleaned and explored using Python 3.9. For preprocessing data, we have used Simple Imputer, Standard Scaler, Ordinal Encoder and Label Encoder from Scikit-learn (Pedregosa et al., 2011). Dimensionality reduction was conducted using Scikit-learn (Pedregosa et al., 2011) library (Principal Component Analysis [PCA], Multidimensional Scaling [MDS], t-distributed Stochastic Neighbor Embedding [TSNE] and Uniform Manifold Approximation and Projection (UMAP) used the UMAP library (McInnes, 2018). For t-SNE we have used number of neighbors of 5, 13 and 45 and minimum distance of 0.01, 0.1 and 0.5. In the case of UMAP we have iterated through perplexity of 5, 20, 50 and 100 and number of iterations of 300, 900, 1,500 and 2,000. Unless otherwise specified, specifications of each algorithm were set for default. Graphics in **Figures 1**, **7**, **8** and **Supplementary Figure S3** were created using Seaborn or MatPlotLib and the remaining ones in GraphPad Prism 8.

Cell Culture Conditions

MRC-5 fibroblasts (European Collection of Authenticated Cell Cultures, Porton Down Salisbury, United Kingdom) were cultured in MEM and SH-SY5Y cells (American Type Culture Collection, LGC Standards S.L.U., Spain) were cultured in DMEM/F-12. Both mediums contained 10% FBS and 1% penicillin/streptomycin and both cell lines were maintained at 37°C with 5% CO_2.

Viability Assays

For viability assessment, MRC-5 fibroblasts were seeded at a density of 2×10^4 cells/well. After 24 h the cells were incubated with the compounds of interest. 24 h later, the wells are aspirated, the medium was replaced by MTT at 0.5 mg/ml and incubated for 2 h. At the end of this period, the solution was discarded and the formazan crystals in the wells dissolved in 200 µL of a 3:1 DMSO: isopropanol solution. The absorbance at 560 nm was read in a Thermo Scientific™ Multiskan™ GO microplate reader.

Results are presented as the percentage of control and correspond to the mean ± SEM of at least three independent experiments, each of them performed in triplicate.

Cytosolic Calcium Level Determination

MRC-5 fibroblasts were plated on black bottomed-96-well plates at the density of 2×10^4 cells/well. After 24 h, the fluorescent probe Fura-2/AM was added at 5 µM and incubated for 1 h. Then these were incubated with the selected nontoxic compounds in HBSS. The calcium ionophore A23187 was added at a final concentration of 5 µM after 2 h. Finally, 2 h later the fluorescence was read at 340/505 and 380/505 nm on a Cytation™ 3 (BioTek (Vermont, MA, United States)) multifunctional microplate reader. Data analysis was performed considering the ratio $F_{340/505}/F_{380/505}$. Results are presented as fold decrease *vs.* positive control and represent the mean ± SEM of at least three independent experiments, each of them performed in triplicate.

RNA Extraction and Quantification, cDNA Synthesis and RT-qPCR Reaction

Cells were seeded at 1.6×10^5 cells/well in 12-well plates, left at 37°C for 24 h and then incubated with the compounds that displayed positive results in previous assays. After 2 h, thapsigargin (Tg) was used as a positive control and added at a final concentration of 3 µM, and a period of 16 h of incubation ensued. The cells were lysed by aspirating the culture medium and adding 500 µL of PureZOL RNA isolation reagent, pipetting up and down multiple times. The lysate was kept at room temperature for 5 min and then RNA extraction ensued.

The extraction was performed by phase separation, by adding 100 µL of chloroform, shaking, incubating for 5 min and centrifuging at 12,000 *g* for 15 min at 4°C. The aqueous phase was collected and 250 µL of isopropyl alcohol were added, following 5 min of incubation and new centrifugation at 12,000 *g* for 10 min, at 4°C. The supernatant was then discarded, and the pellet was washed with 75% ethanol, vortexed, centrifuged at 7,500 *g* for 5 min at 4°C, air dried and resuspended in DEPC-treated water. The RNA in the sample was quantified resorting to the Qubit® RNA HS assay kit. Sample integrity was then evaluated with the Qubit® RNA IQ assay kit, and, if in appropriate conditions, 1 µg was converted to cDNA using the SuperScriptTM IV VILO™ MasterMix.

RT-qPCR reaction was performed in the following thermal cycling conditions: 3 min at 95°C, 40 cycles of 95°C for 3 s (denaturation), gene-specific temperature for 20 s (annealing temperatures listed on **Table 1**) and 20 s at 72°C (extension). The employed mastermix was KAPA SYBR® FAST qPCR Kit Master Mix (2X) Universal. The reaction was conducted on a qTOWER3 G (Analytik Jena AG, Germany), and the data were analyzed on the software supplied along with the equipment (qPCRsoft 4.0). Primers for target genes were designed on Primer BLAST (NCBI, Bethesda, MD, United States) and synthesized by Thermo Fisher (Waltham, MA, United States). The respective nucleotide sequences are presented on **Table 1**. Product specificity was checked with melting curves. GAPDH was selected as reference genes for normalization of expression. All the RT-qPCR reactions were performed in duplicate, and the experiments were repeated, at least, four times. Results are presented as mean ± SEM.

Quantification and Imaging of Protein Aggregates

On black bottomed-96-well plates, MRC-5 and SH-SY5Y cells were seeded at the densities of 2×10^4 and 3×10^4 cells/well, respectively. In the following day, they were incubated with the selected molecules in the presence of $A\beta_{25\text{-}35}$ at 10 µM. After an incubation period of 24 h, cells were washed with HBSS and incubated for 30 min with thioflavin T at 5 µM (prepared in HBSS). At this point, fluorescence was read at 450/482 nm on a CytationTM 3 (BioTek (Vermont, MA, United States)) multifunctional microplate reader. Results represent the fold decrease on fluorescence compared to the positive control. We present the mean ± SEM of, at least, three independent assays, individually performed in triplicate.

To image protein aggregates, cells were seeded on clear bottomed-96-well plates at the aforementioned density and treated with the molecules of interest for 24 h in the presence of $A\beta_{25\text{-}35}$ at 10 µM. Cells were fixed on 4% formaldehyde at room temperature for 15 min and incubated with 10 µM thioflavin T

TABLE 1 | Data concerning analyzed genes and designed primer sequences.

Gene	Accession Number	Primers	Annealing temperature (°C)	Amplicon Length (Bp)
GAPDH (GAPDH)	NM_002,046.6	F: AGGTCGGAGTCAACGGATTT R: TGGAATTTGCCATGGGTGGA	60	157
HSPA5 (GRP78)	NM_005,347.4	F: ACTCCTGAAGGGGAACGTCT R: TTTTCAACCACCTTGAACGGC	59.5	161
DDIT3 (CHOP)	NM_001195053.1	F: AAGTCTAAGGCACTGAGCGT R: TTGAACACTCTCTCCTCAGGT	59	93
HSP90B1 (GRP94)	NM_003,299.2	F: GCTCTATGTGCGCCGTGTAT R: ATCTGAGTCCACCACACCCTT	60.5	91
ATF4 (ATF4)	NM_001,675.4	F: ACAACAGCAAGGAGGATGCC R: CCAACGTGGTCAGAAGGTCA	60	135
EDEM1 (EDEM1)	NM_014,674.2	F: GCGGGGACCCTTCAAATCT R: CGGCTTTCTGGAACTCGGAT	60	117

for 60 min. The counter staining was performed with DAPI at 0.25 μg/ml, for 30 min. Finally, three washing steps with HBSS for 5 min were carried out and cells were imaged under an Eclipse Ts2R-FL (Nikon) fluorescence microscope equipped with a Retiga R1 camera. A FITC filter was employed to observe thioflavin T and DAPI staining was imaged using a DAPI filter. Images were analyzed resorting to the CellProfiler software version 4.2.1 (Broad Institute of MIT and Harvard, Cambridge, MA).

Western Blotting Analysis

MRC-5 and SH-SY5Y cells were seeded in 6-well plates at the densities of 3.2×10^5 and 4.8×10^5 cells/well. After 24 h, they were incubated with compounds selected as promising in previous experiments. After 2 h, Tg at 3 μM was added, and the plates were left in the incubator for another 22 h. By the end of this time frame, cell samples were lysed in RIPA buffer containing 1% protease inhibitor cocktail and 1% phosphatase inhibitor cocktail for 15 min at 4°C, and subsequently centrifuged at 14,000 *g* for 15 min to remove cell debris. The supernatant was then collected, and the protein content was determined resorting to the Qubit® Protein Assay Kit.

The following step was to submit 30 μg of each sample, previously denatured at 76°C for 10 min, to 10% SDS-PAGE electrophoresis, in a gel containing 10% acrylamide/bisacrylamide. The proteins were then transferred to a nitrocellulose membrane on a Trans-Blot® Turbo (Bio-Rad; Hercules, CA, United States). The membrane was blocked in a PBS solution containing 5% non-fat milk and 0.1% Triton X-100 for 1 h with orbital agitation. Hereupon, the membrane was incubated with the primary antibody overnight, at 4°C, with agitation. The anti-BiP mouse monoclonal antibody was used at a working dilution of 1:1,250, while the anti-GAPDH rabbit monoclonal antibody was used at a dilution of 1:10,000. A washing step was then performed with PBS 0.1% Triton X-100 for 30 min. Then, the secondary antibody was incubated for 2 h at room temperature. The anti-mouse secondary antibody was used at 1: 2,000, and the anti-rabbit secondary antibody at 1:3,000. At this point, two more washing steps were performed with PBS 0.1% Triton X-100 for 15 min and then with PBS, again twice for 15 min. Finally, bands were detected by addition of a chemiluminescent substrate, WesternBright ECL HRP. The resulting bands were visualized on a ChemiDoc™ Imaging System (Bio-Rad, Hercules, CA, United States). Their relative optical density was calculated by densitometry resorting to the Fiji/ImageJ software version 1.51 (Fiji, Madison, WI, United States) and normalized against the loading control (GAPDH). Results are presented as mean ± SEM of, at least, three independent experiments.

Statistical Analysis

The statistical analysis was performed using GraphPad Prism 8 software. We resorted to unpaired Student's t-tests to compare every single individual treatment to the control group. Values of $p < 0.05$ were considered statistically significant. Outliers were identified and excluded by the Grubbs' test.

RESULTS

Chemical Space of the Library

We compiled a library of 134 molecules of natural origin (**Supplementary Table S2**). The average molecular weight was 358 g/mol, the inferior limit being 110.1 g/mol (catechol and *p*-hydroquinone) and the upper limit 1,131.3 (β-escin) (**Figure 1**). The computed natural product-likeness score, a parameter that tries to quantify how much a given molecule is "natural product-like" (Vanii Jayaseelan et al., 2012) had an average of 1.29 (min: 0.4, max: 2.72, **Figure 1**). Over 50% of the molecules displayed no violations of Lipinski's Rule of 5 with over 30% displaying 2 or more (**Figure 1**), a relevant trait for candidate drugs.

For chemical ontology, we have used the computed chemical classes generated by ClassyFire (Djoumbou Feunang et al., 2016). From a chemical point of view, the distribution of the molecules by chemical superclass can be found in **Figure 1**. Phenylpropanoids and polyketides corresponded to the majority of the entries (65.9%), followed by benzenoids (14.4%) and lipids or lipid-like molecules (6.1%). Within phenylpropanoids, flavonoids were the most prevalent molecules (**Figure 1**), followed by cinnamic acids and their derivatives. In the case of benzenoids, simple phenols were predominant, while in the case of lipids, prenol lipids were the most representative (**Figure 1**). The chemical structures of all of the molecules are represented in **Supplementary Figure S1**, separated according to the herein mentioned chemical superclasses.

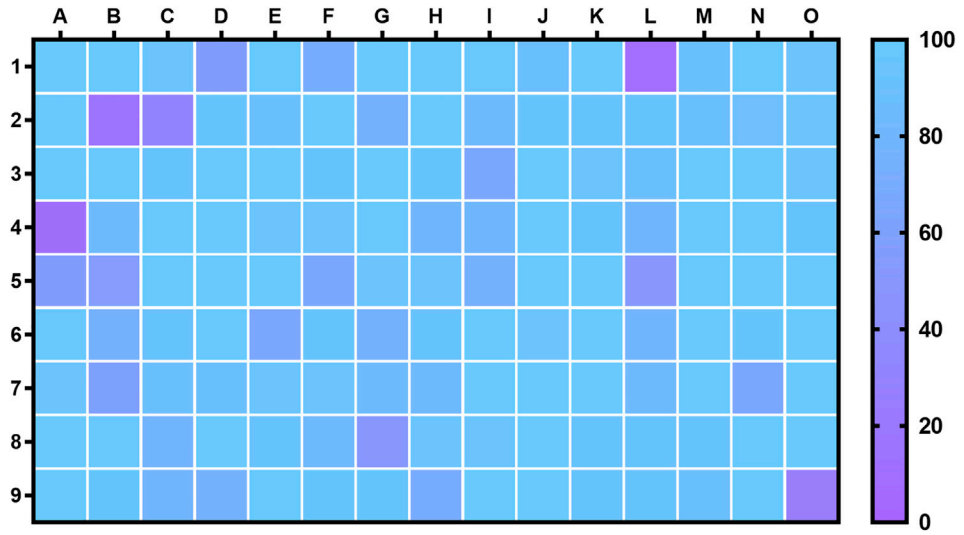

FIGURE 2 | Impact of a library of natural products on MRC-5 fibroblasts viability, as determined by MTT reduction assays. Results represent the percentage of the control and correspond to, at least, three independent experiments, each performed in triplicate.

Impact of Molecules Upon Cell Viability

Given the high number of molecules involved, all compounds were tested at a single concentration (50 μM). Statistically significant decreases in MTT reduction were interpreted as negative impact on cellular viability and the corresponding molecules excluded from subsequent experiments. As evidenced by **Figure 2**, 37 molecules (depicted in **Supplementary Table S2**) were dropped from the pipeline for their toxicity.

The remaining 97 compounds were screened for potential protective capacity against ER stress. The legend for the heatmap presented in **Figure 2** can be consulted in **Supplementary Table S2**, while **Supplementary Figure S2** contains the individual results for each molecule represented in the bar charts.

Effect of the Library Upon Cytosolic Calcium Levels

The next step involved the screening of the nontoxic molecules for potential protection against the onset of ER stress. Towards this goal, and considering the high number of molecules still in the pipeline, we selected changes on calcium levels as an indicator of compromised ER homeostasis. The maintenance of the high concentration of calcium in the ER lumen creates an appropriate environment for protein folding, and thus changes on its levels heavily impact ER function (Kraus and Michalak, 2007; Carreras-Sureda et al., 2018). This organelle is able to maintain its calcium levels due to the abundance of resident calcium-buffering proteins, like calnexin and calreticulin (Coe and Michalak, 2009). Under stress conditions, the ER may release calcium through channels, such as IP_3R and RyR. Eventually, this may lead to increased calcium in mitochondria, indirectly inducing the generation of ROS and triggering the dissipation of the mitochondrial membrane potential, ultimately leading to the release of resident proapoptotic factors (Bhattarai et al., 2021).

To evaluate the potential protective effect of the molecules under study, we conducted experiments with the fluorescent probe Fura-2/AM. Calcium ions were detected employing the divalent cation ionophore A23187 (5 μM) as a positive control for calcium leakage into the cytosol and molecules that could inhibit or counter its effect were searched. Calcium ionophore A23187, or calcimycin, is a calcium-binding molecule that increases the cellular permeability of ionic calcium (Verma et al., 2011). There are multiple examples in the literature of the use of this molecule to increase cytosolic calcium levels, inducing ER stress, UPR activation and eventual apoptosis or autophagy (Castillero et al., 2015; Jung et al., 2015; Shinde et al., 2016).

Under these experimental conditions, we were able to identify several molecules that significantly prevented or ameliorated the calcium overload caused by A23187, as displayed in **Figure 3**. Such molecules included six polyphenols (5-deoxykaempferol, delphinidin, fisetin, naringenin, naringin, quercetin-3-*O*-β-D-glucoside), one anthraquinone (sennoside B), one fatty acid (myristic acid) and one biogenic polyamine (spermine). The full list of molecules tested in this assay can be consulted in **Supplementary Table S3**, while **Supplementary Figure S3** represents these data in the bar charts.

ER Stress Counter Candidates Inhibit Thapsigargin-Induced UPR Signaling in MRC-5 Fibroblasts

The non-toxic molecules that successfully lowered Ca^{2+} levels were considered potential candidates for countering ER stress. As so, they were evaluated for their effect upon UPR signaling pathways.

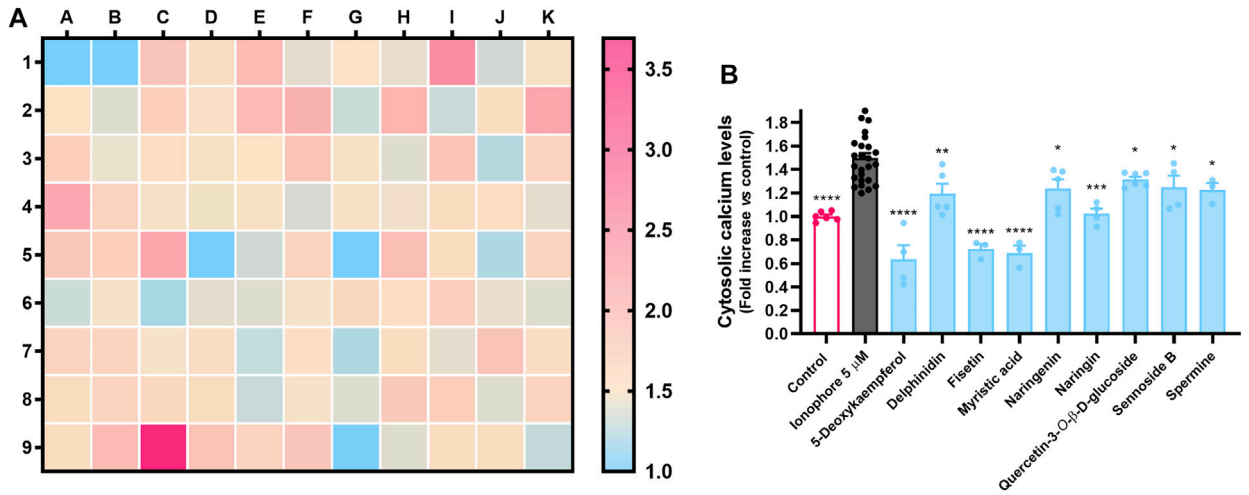

FIGURE 3 | Cytosolic calcium levels in MRC-5 fibroblasts in response to co-incubation of calcium ionophore A23187 at 5 μM and nontoxic molecules (50 μM), as determined by the fluorescence of the probe Fura-2/AM. **(A)** Heatmap representing all molecules tested; **(B)** Molecules that caused a statistically significant decrease in calcium levels when compared to the positive control. Results correspond to the mean of, at least, three independent experiments, each performed in triplicate.

Thapsigargin, a natural sesquiterpene lactone that is widely used as UPR inducer, was the positive control. This molecule acts as an irreversible SERCA pump inhibitor, leading to an impaired calcium homeostasis and subsequent onset of organized cell death mechanisms (Pereira et al., 2015). Accordingly, as evidenced by **Figure 4**, we can see that thapsigargin (3 μM) significantly increased the expression of all the genes of interest, namely the transcription factors *DDIT3* and *ATF4*, the chaperones *HSPA5* and *HSP90B1* (BiP and GRP94 proteins, respectively), and *EDEM1*, a gene coding for the ER degradation-enhancing alpha-mannosidase-like protein 1, an enzyme involved in ER-associated degradation.

5-Deoxykaempferol at 50 μM inhibited the expression of *DDIT3*, *HSP90B1*, *EDEM1* and *HSPA5*, even though it did not significantly decrease *ATF4* expression. Fisetin was the only molecule to prevent the increase of all target genes in a significant manner. Delphinidin negatively impacted the expression of *ATF4*, *HSP90B1* and *EDEM1*. Myristic acid and quercetin-3-*O*-β-D-glucoside displayed a similar pattern in the protection against UPR activation, by modulating *HSP90B1* and *EDEM1* expressions. Sennoside B acted upon *ATF4* and *EDEM1*, while naringenin, naringin and spermine failed to inhibit any of the selected genes.

Molecules That Counter ER Stress Ameliorate Protein Aggregation in MRC-5 Fibroblasts and Attenuate UPR Activation at the Protein Level

As discussed earlier, activation of the UPR affects the capacity of cells to fold proteins properly, which frequently results in the formation of protein aggregates and may lead to proteinopathies (Doyle et al., 2011; Ogen-Shtern et al., 2016). Conversely, several diseases, notably those of neurodegenerative nature, are associated with these aggregates (Kim et al., 2016). As so, new molecules capable of countering ER stress are expected to be able to prevent or lower the amounts of protein aggregates in a biological context. To confirm this, we proceeded to an experimental model of ER stress-triggered protein aggregation using $A\beta_{25-35}$ as a protein aggregation inducer. $A\beta_{25-35}$ is an active fragment of $A\beta_{42}$ (Zhou et al., 2016), a peptide that is associated to the pathogenesis of Alzheimer's disease (AD) and has been characterized in experimental models, where it can lead to the formation of protein aggregates *in vitro* and AD *in vivo* (Liu et al., 2017).

As shown in **Figure 5A**, incubation of MRC-5 cells with $A\beta_{25-35}$ elicits protein aggregation, as assessed with thioflavin T, a benzothiazole that presents high fluorescence when bound to β-sheet-rich structures common in protein aggregates, both in a microplate-based (**Figure 5A**) and an imaging method (**Figure 5B**). In the same conditions, delphinidin, fisetin, myristic acid, sennoside B and quercetin-3-*O*-β-D-glucoside significantly inhibited this effect.

Our Western blotting results show that the exposure of Tg-insulted MRC-5 cells to delphinidin and fisetin clearly reduced BiP expression, and, consequently, we presume that the UPR activation in the presence of these molecules is mitigated.

Selected Molecules Counter Protein Aggregation and UPR Activation at the Translational Level in Neuronal Cells

For this assay, the concentrations of the molecules under study had to be adjusted to the highest nontoxic concentration towards this cell line. Fisetin was tested at 25 μM, while delphinidin was tested at the concentration used in MRC-5 cells (50 μM). The effect of fisetin was not replicated on SH-SY5Y cells. We hypothesize that this may be due to the reduction of the

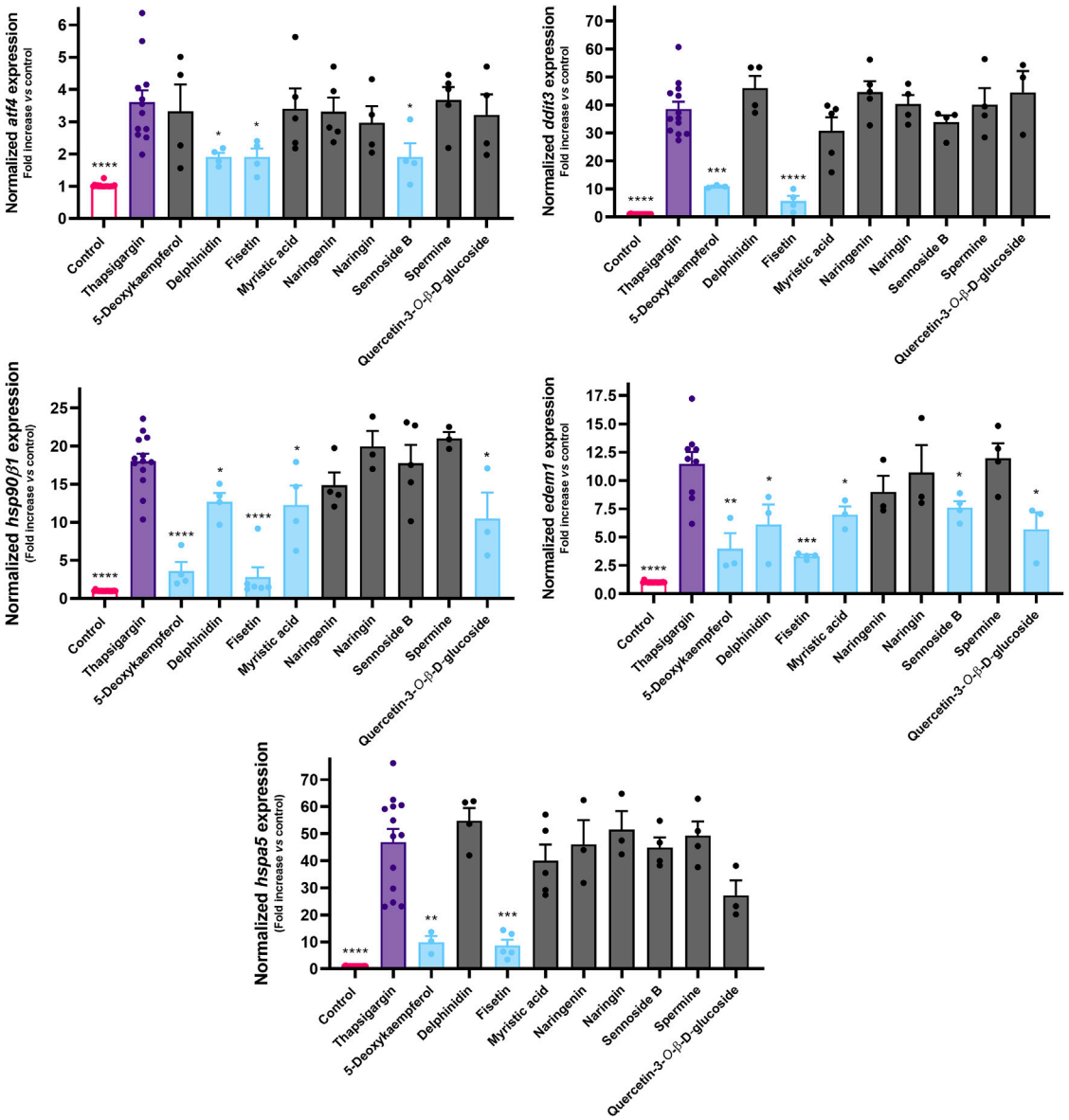

FIGURE 4 | Effect of 5-deoxykaempferol, delphinidin, fisetin, myristic acid, naringenin, naringin, sennoside B, spermine and quercetin-3-*O*-β-D-glucoside on Tg-induced UPR signaling, as determined by RT-qPCR. Results correspond to the mean ± standard error of the mean of, at least, four independent experiments, each performed in duplicate. *GAPDH* was used as a reference gene for normalization of expression.

concentration that was necessary in order not to impact cell viability in this model. On the other hand, the effect of delphinidin translates to these cells, virtually nullifying the advent of protein aggregates, as evidenced by **Figures 6A,B**.

Defining a Chemical Space for Future Drug Development

Considering all the information generated during this work, together with the chemical, structural and topographical information available for the molecules under study, we were interested in understanding if the physico-chemical properties of the library could, *per se*, be a good indicator for its activity. To this end, we took all the molecules used and computed multiple pairs of their properties, sorting them as active or inactive according to the results of the aggregation assays depicted in **Figure 5**. While there seemed to be a tendency of active molecules to be apart from inactive molecules in some cases (**Supplementary Figure S4**), it soon became apparent that a pairwise comparison could leave behind important features of the molecules, as it reduces high dimensional data to just two dimensions. As

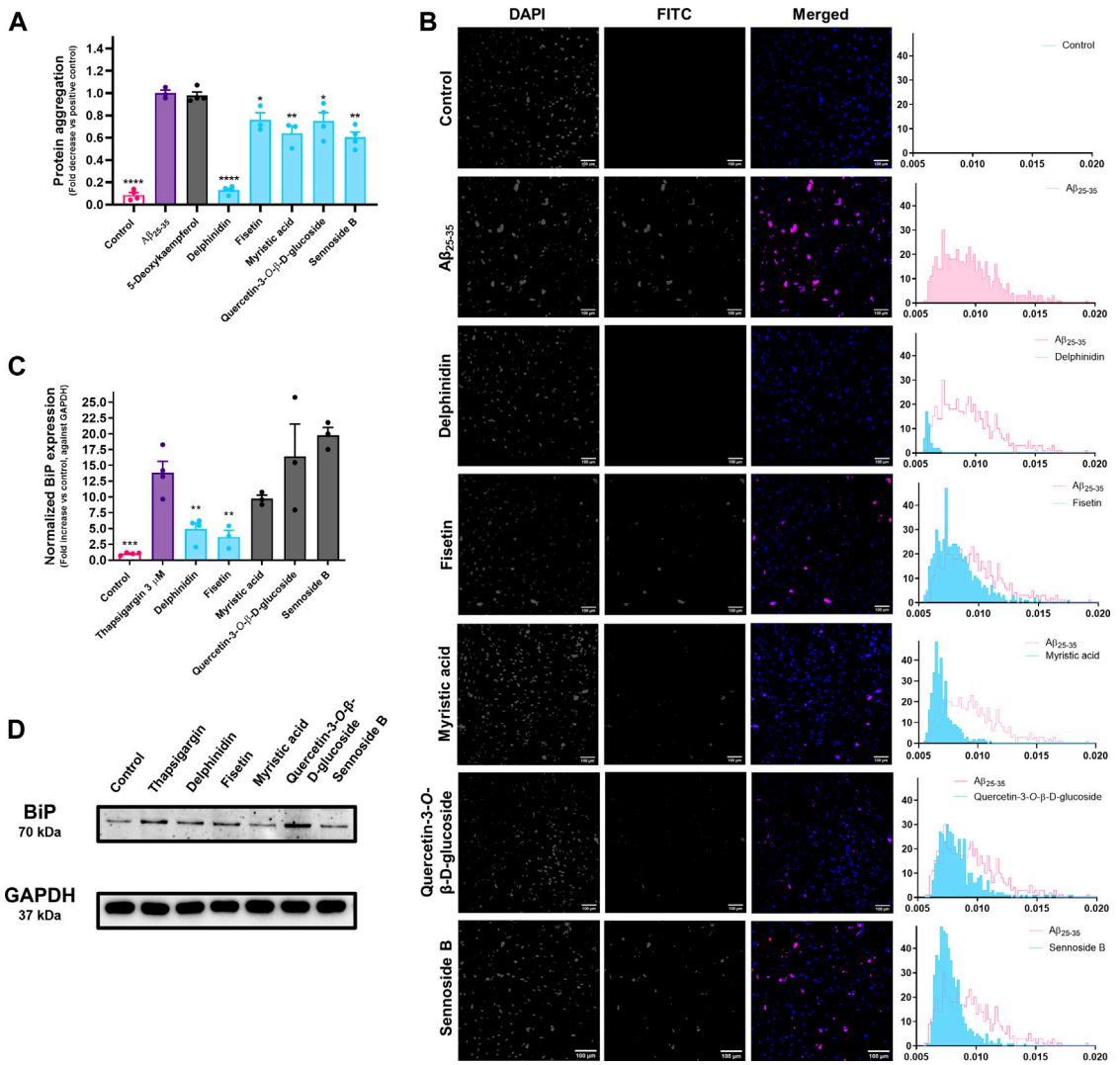

FIGURE 5 | (A) Impact of delphinidin, fisetin, myristic acid, sennoside B and quercetin-3-*O*-β-D-glucoside on $A\beta_{25-35}$-induced protein aggregation in MRC-5 cells, determined by the fluorescence of thioflavin T. Results correspond to the mean ± standard error of the mean of, at least, three independent experiments, individually performed in triplicate. **(B)** The protective effect of bioactive molecules was captured under a fluorescence microscope. The fluorescence signal of thioflavin T is represented in the histograms. **(C)** Effect of delphinidin on Tg-induced BiP expression in MRC-5 cells, as evaluated by Western blotting. Results correspond to the mean ± standard error of the mean of, at least, three independent experiments. **(D)** Images obtained through Western blotting analysis.

so, we have decided to use other methodologies that could take into account all the features of the library, namely dimensionality reduction algorithms, which allows the combination of different features into principal components that can be more easily graphed and understood. We first conducted a correlation study in order to identify molecular features that were highly correlated, which could negatively impact the performance of the statistical analysis given the redundancy it would add. **Figure 7** shows the original features, where it is clear that many are highly correlated, for example, the features "total atom number" and "number of carbons" (0.98), as one directly affects the other. Such features were dropped, and the remaining ones were used. We also decided to assess the robustness of the methods in identifying the chemical space occupied by the molecule that was shown to be active in both cell lines, namely delphinidin.

We initially used the classical algorithm for principal component analysis (PCA), which is widely used both for chemometric and biological data (Meglen, 1992; Boileau et al., 2020). As shown, PCA was unable to identify a chemical space occupied solely by the molecule that was shown to be active in all the assays used (**Figure 8A**), the same being true for multidimensional scaling (MDS, **Figure 8B**). In light of this, we applied a suite of other algorithms, both individually and in tandem with PCA, namely uniform manifold approximation and projection (UMAP) and t-distributed stochastic neighbor embedding (t-SNE).

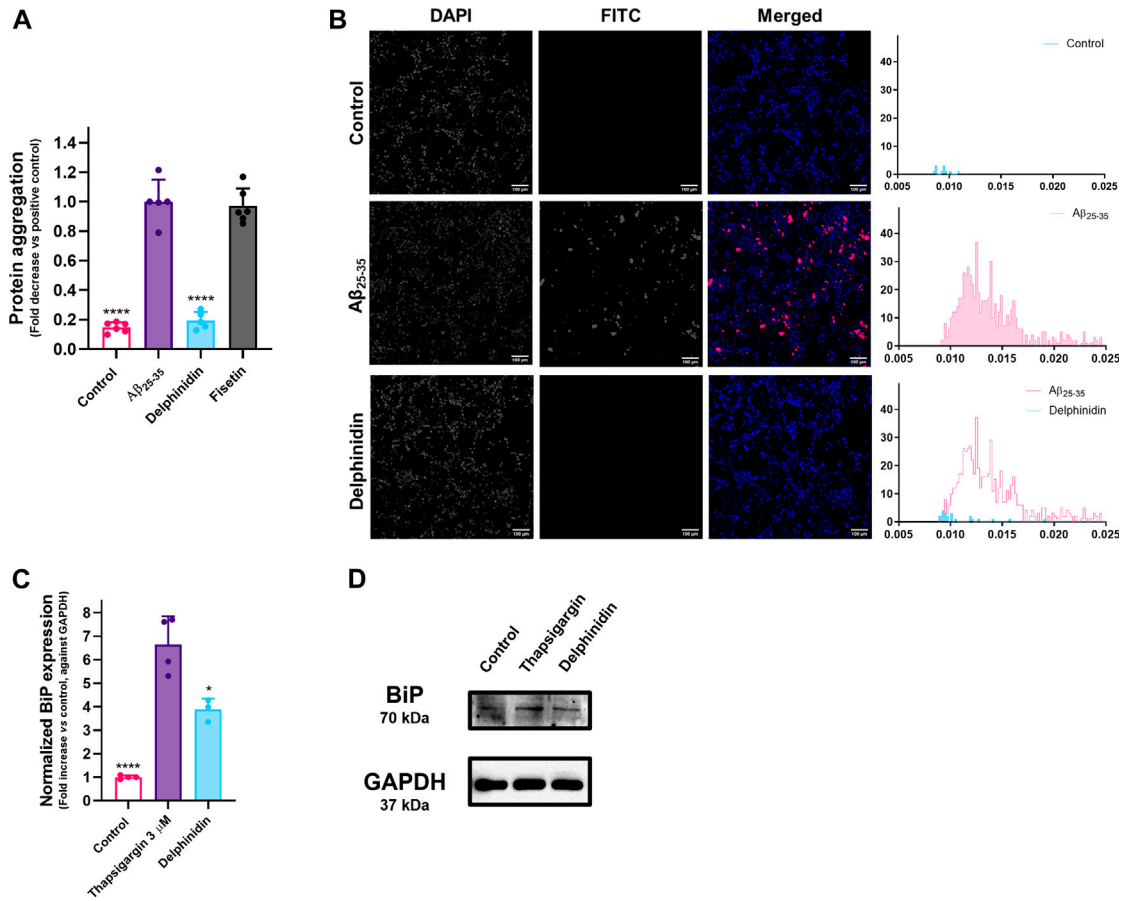

FIGURE 6 | (A) Effect of delphinidin and fisetin on $A\beta_{25-35}$-induced protein aggregation in SH-SY5Y cells, as evaluated by determination of the fluorescence of thioflavin T. Results correspond to the mean ± standard error of the mean of, at least, three independent experiments, each performed in triplicate. **(B)** The effect of bioactive molecules was observed under a fluorescence microscope. The fluorescence signal of thioflavin T is represented in the histograms. **(C)** Effect of delphinidin on Tg-induced BiP expression in SH-SY5Y cells, as evaluated by Western blotting. Results correspond to the mean ± standard error of the mean of, at least, three independent experiments. **(D)** Example of the obtained Western blotting results.

Differently from PCA and MSD, the combined use of PCA + UMAP led to 2-principal component-based space, in which delphinidin clearly occupies an outlier space. We have tried distinct combinations of parameters, as stated in the Materials section, the number of neighbors of 45 giving the best performance, both for minimum distance of 0.01 and 0.1. In order to confirm this result, we have employed an additional algorithm, namely PCA + t-SNE. Again, it was shown that delphinidin, together with an outlier, occupies a space that is distinct from over 98% of the library.

DISCUSSION

Having performed the characterization of our in-house library of over 130 natural products, considering that new candidates for countering ER stress should be devoid of toxicity, we proceeded to the evaluation of the impact of all the molecules in the viability of fibroblasts, as assessed by the MTT reduction assay. Fibroblasts present a highly developed endoplasmic reticulum, since their function relates to the production of components of the extracellular matrix, and thus are particularly susceptible to ER stress, reason for which they were chosen as experimental model in this work (Weidner et al., 2018).

The maintenance of the high concentration of calcium in the ER lumen creates an appropriate environment for protein folding, and thus changes on its levels heavily impact ER function (Kraus and Michalak, 2007; Carreras-Sureda et al., 2018). This organelle is able to maintain its calcium levels due to the abundance of resident calcium-buffering proteins, like calnexin and calreticulin (Coe and Michalak, 2009). Under stress conditions, the ER may release calcium through channels, such as IP_3R and RyR. Eventually, this may lead to increased calcium in mitochondria, indirectly inducing the generation of ROS and triggering the dissipation of the mitochondrial membrane potential, ultimately leading to the release of resident proapoptotic factors (Bhattarai et al., 2021). We were able to identify molecules with the capacity to

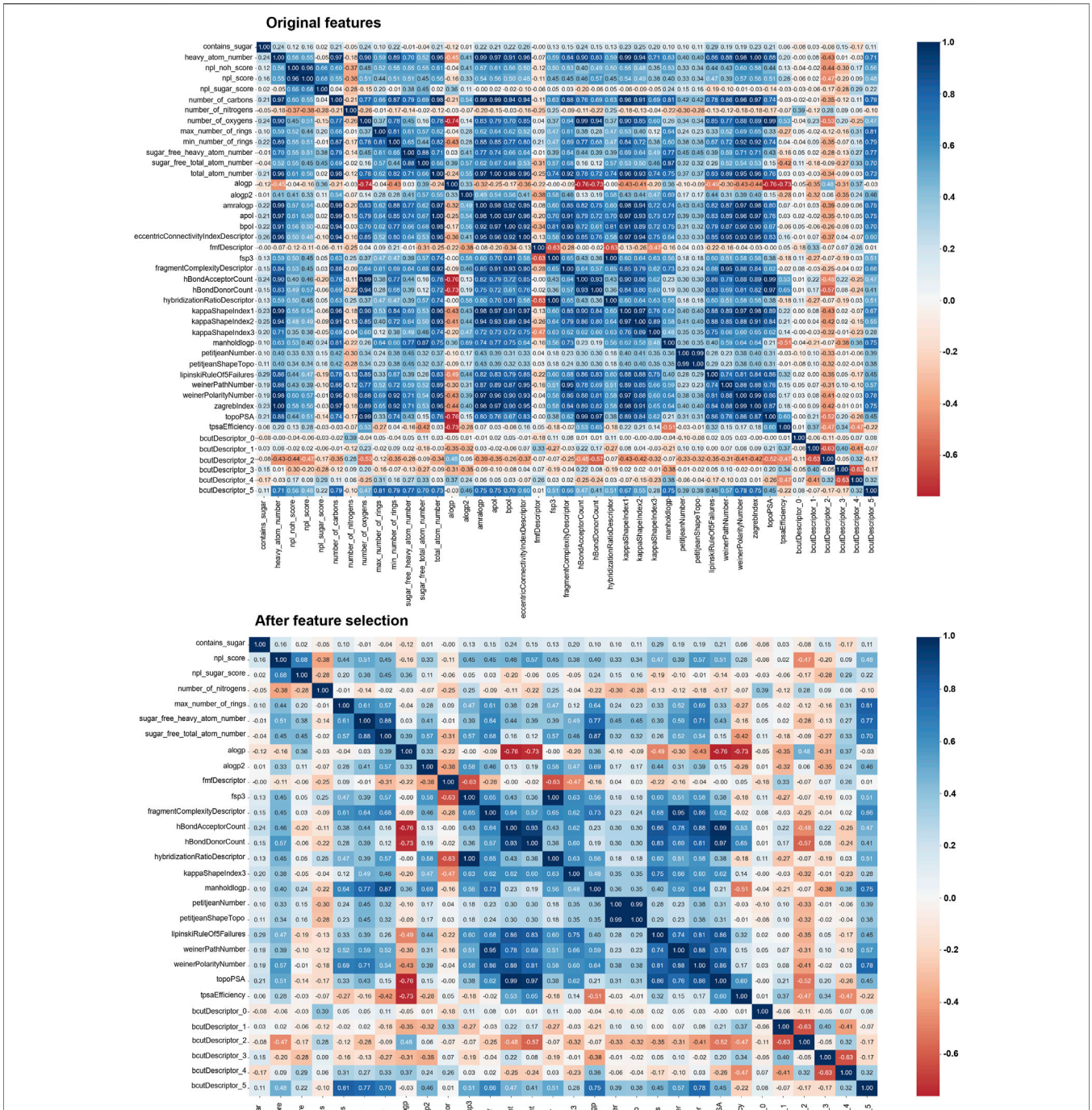

FIGURE 7 | Correlation matrix for the features used for the chemical library used in this work.

ameliorate ionic calcium leakage into the cytosol, namely 5-deoxykaempferol, delphinidin, fisetin, naringenin, naringin, quercetin-3-*O*-β-D-glucoside, sennoside B, myristic acid and spermine, and thus deemed these molecules with potentially protective against ER stress, and selected them to subsequent assays.

Regarding the RT-qPCR results, we show that 6 out of the 9 molecules that effectively countered the calcium overload were,

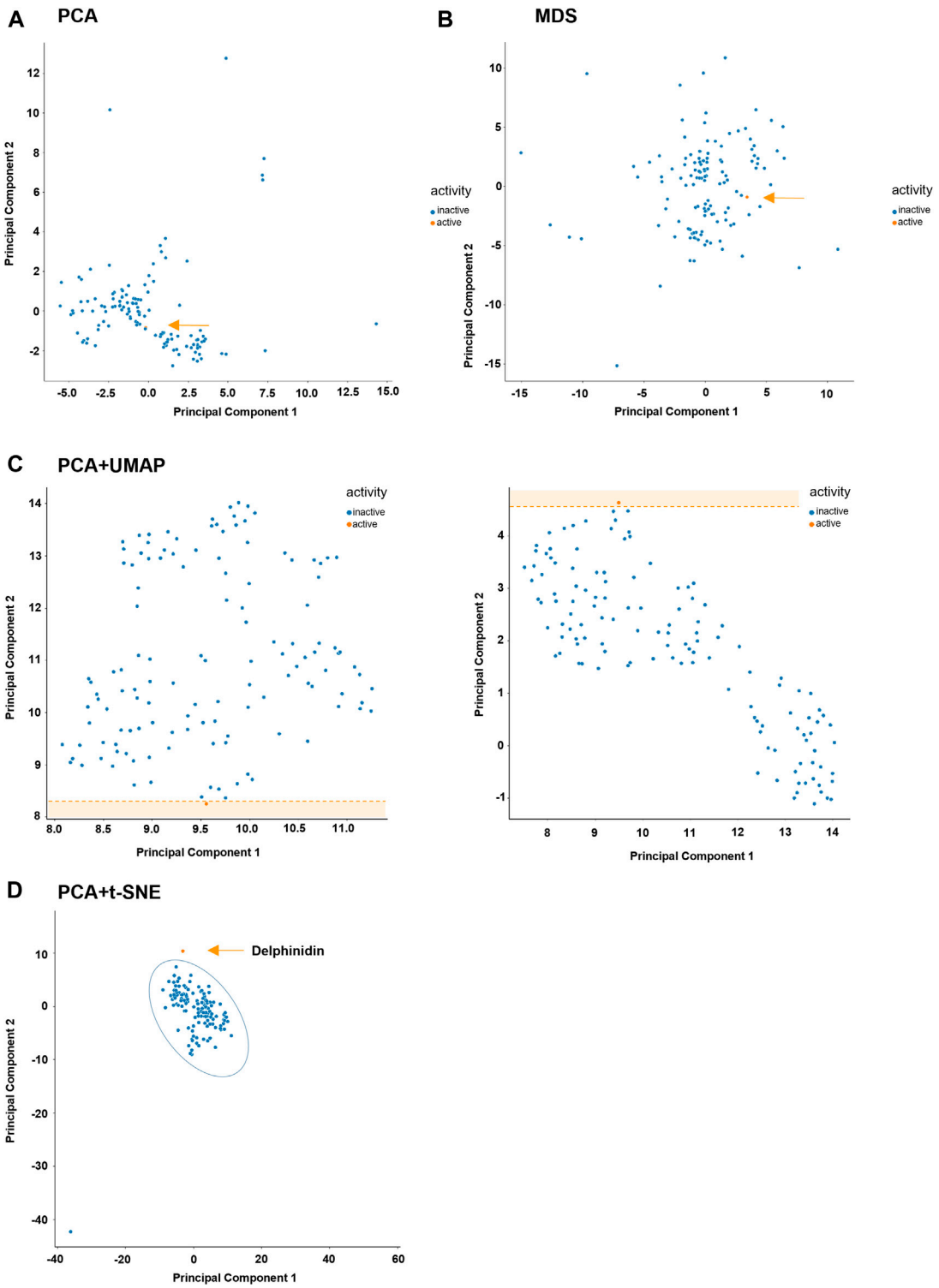

FIGURE 8 | Different dimensionality reduction methods applied to chemical library under study. The active molecule delphinidin is presented in orange and inactive molecules in blue. **(A)** variation explained: 0.9. **(B)** number of components: 2, metric MDS, max_iterations=300. **(C: left)** number of neighbors: 45; minimum distance: 0.01. **(C: right)** number of neighbors: 45; minimum distance: 0.1. **(D)** perplexity: 50; number of iterations: 300.

simultaneously, capable of downregulating UPR-associated genes, which suggests that the assessment of cytosolic calcium levels is a reliable method to screen for the capacity to counter ER stress in this experimental model. Considering that 5-deoxykaempferol, delphinidin, fisetin, myristic acid, sennoside B and quercetin-3-*O*-β-D-glucoside were capable of significantly preventing Tg-induced increased expression of, at least, two UPR-related genes, they were selected for subsequent studies. Among these molecules, fisetin displayed the strongest bioactivity at the mRNA expression level since it significantly inhibited the expression of all target genes. In contrast, naringin, naringenin and spermine failed to inhibit the expression of any of the analyzed genes, thus they were dropped from the pipeline.

Taking into account that increased UPR-related gene expression characterizes ER stress, many natural products have been described as ER stress modulators (either inducers or inhibitors) upon observation of their impact on the expression of these genes (Pereira et al., 2015). Most of the molecules that here displayed the potential to ameliorate UPR signaling have not been described before as ER stress modulators. However, fisetin has already been reported as an ER stress inhibitor, reducing *HSPA5* (BiP) mRNA expression in hepatocytes (Dai et al., 2022). Relevantly, fisetin has already been described as neuroprotective by inhibition of protein aggregation and neuroinflammation in mice (Ahmad et al., 2017). There are also several reports of its bioactivity as an UPR inducer in different contexts (Kang et al., 2016; Jia et al., 2019).

On MRC-5 fibroblasts, we show that the molecules that had been selected on the basis of their ability to attenuate UPR pathways were able to act upon the endpoint biological effect of this cascade, namely protein aggregation. As mentioned before, the UPR relies on three major signaling branches. They are all governed by the major chaperone BiP, coded by the gene *HSPA5*. Under homeostatic conditions, BiP remains bound to the three major UPR players (PERK, IRE1 and ATF6), releasing them whenever it recognizes the presence of misfolded proteins. This extends the permanence of these proteins in the ER lumen, in order to promote their correct processing. For these reasons, BiP is a key regulator of UPR signaling and its activation prevents protein aggregation (Gorbatyuk and Gorbatyuk, 2013). In light of our results, we conclude that the UPR activation in the presence of delphinidin and fisetin is mitigated, as they clearly reduced BiP expression. Since both molecules significantly decreased the occurrence of protein aggregates in the cells, we conclude that the observed BiP levels, closer to the basal levels of the control group, are a consequence of a decreased UPR activation. This implies that ER stress levels on the presence of a stress inducer are restored by the presence of delphinidin or fisetin, whether the inducer is thapsigargin or protein aggregation. We can therefore assume that both molecules contribute to a homeostatic protein folding environment in the ER lumen.

It is described that the expression of this chaperone is increased throughout the course of neurodegenerative disease (Ghemrawi and Khair, 2020). In human brains of AD patients, a significant increase in BiP expression was observed when compared to samples of non-demented patients (Hamos et al., 1991; Hoozemans et al., 2005). It is known that this increased expression emerges early in the pathogenesis of AD and, at this stage, correlates with the adaptive response of the UPR; however, the sustained UPR activation that underlies the disease results in neurodegeneration (Hoozemans et al., 2009). Additionally, there is considerable amount of evidence indicating the neuroprotective effect of UPR inhibition (Moreno et al., 2013; Halliday et al., 2015; Radford et al., 2015). This is, to the extent of our knowledge, the first report of the protective effect of delphinidin against ER stress and UPR activation.

Given the promising results on MRC-5 fibroblasts, we repeated the experiment, this time with SH-SY5Y cells, in order to analyze whether these compounds could also be protective on this neuronal cell line. The SH-SY5Y cell line has been widely used and described as a good *in vitro* model for the study of protein aggregation (Nonaka et al., 2010; Rcom-H'cheo-Gauthier et al., 2017; Xicoy et al., 2017; Sang et al., 2021), a process that has been shown to be both consequence and cause of misfolded proteins in the ER and subsequent activation of the UPR (Roussel et al., 2013). Relevantly, in the case of AD it has been shown that increased levels of phosphorylated PERK and IRE1α are found in the hippocampus of the patients and that they colocalize with phosphorylated tau. Furthermore, treatment of cells with $A\beta_{42}$, the major component of amyloid plaques, induces CHOP expression, which is a product of the PERK and ATF6 branches of the UPR (Lee et al., 2010; Santos and Ferreira, 2018; Ghemrawi and Khair, 2020). The literature already conveys reports of the bioactivity of naturally occurring small molecules as pharmacological chaperones, for instance, flavonoid glycosides that were protective against protein aggregation in cell-based experiments (Sharma et al., 2021). In murine cells, a study of over 200 naturally occurring molecules of discrete chemical classes concluded that flavonoids displayed the strongest potential to decrease the formation of protein aggregates in the context of AD (Kim et al., 2005).

The final step in this work was the attempt to define a chemical space where to search for bioactive molecules. Again, it was shown that delphinidin, together with an outlier, occupies a space that is distinct from over 98% of the library. Taken together, these results show that chemometric tools, in tandem with biological data generated from significant number of samples, can be used for future selection of drug candidates relying on data science-based approaches. As so, the composition of the principal components identified can be used for the subsequent selection of novel molecules capable of countering ER stress by screening large databases of molecules for ideal chemical descriptors.

Our framework blending data science-based methods to biological data resulted in the identification of several potentially active molecules against the onset of ER stress. Delphinidin stood out as the most promising candidate against UPR activation and protein aggregation in a cellular model of neurodegenerative disease, being capable to simultaneously

modulate calcium levels and downregulate UPR pathways with meaningful biological endpoints.

In light of our results, it is safe to assume that the natural product chemical space may provide molecules that ultimately lead to the development of novel pharmacological strategies to counter ER stress-related pathologies, as is the case of neurodegenerative diseases.

DATA AVAILABILITY STATEMENT

The original contributions presented in the study are included in the article/**Supplementary Material** and further inquiries can be directed to the corresponding author.

AUTHOR CONTRIBUTIONS

DC has contributed to the implementation of the employed methodologies, performance of experiments, formal data analysis and manuscript preparation. PV supervised the planning of the research activities and performed critical revision of the manuscript. PA contributed with some resources. DP has been responsible for the conceptualization of this work, performed formal analysis and data curation, supervised the planning and execution of the research activities, was involved in the creation of the original manuscript and obtained financial support. All authors approve of the final version to be published.

FUNDING

The work was supported through the project UIDB/50006/2020, funded by FCT/MCTES through national funds. DC extends special thanks to the Fundação para Ciência e Tecnologia (FCT) for the grant (SFRH/BD/130998/2017). The fluorescence microscope was acquired under EU-PRIMA (H2020-Prima 2018 Section 2, Project MILKQUA).

SUPPLEMENTARY MATERIAL

The Supplementary Material for this article can be found online at: https://www.frontiersin.org/articles/10.3389/fphar.2022.956154/full#supplementary-material

REFERENCES

Ahmad, A., Ali, T., Park, H. Y., Badshah, H., Rehman, S. U., and Kim, M. O. (2017). Neuroprotective Effect of Fisetin against Amyloid-Beta-Induced Cognitive/synaptic Dysfunction, Neuroinflammation, and Neurodegeneration in Adult Mice. *Mol. Neurobiol.* 54 (3), 2269–2285. doi:10.1007/s12035-016-9795-4

Bhattarai, K. R., Riaz, T. A., Kim, H.-R., and Chae, H.-J. (2021). The Aftermath of the Interplay between the Endoplasmic Reticulum Stress Response and Redox Signaling. *Exp. Mol. Med.* 53 (2), 151–167. doi:10.1038/s12276-021-00560-8

Boileau, P., Hejazi, N. S., and Dudoit, S. (2020). Exploring High-Dimensional Biological Data with Sparse Contrastive Principal Component Analysis. *Bioinformatics* 36 (11), 3422–3430. doi:10.1093/bioinformatics/btaa176

Carreras-Sureda, A., Pihán, P., and Hetz, C. (2018). Calcium Signaling at the Endoplasmic Reticulum: Fine-Tuning Stress Responses. *Cell. Calcium* 70, 24–31. doi:10.1016/j.ceca.2017.08.004

Castillero, E., Akashi, H., Pendrak, K., Yerebakan, H., Najjar, M., Wang, C., et al. (2015). Attenuation of the Unfolded Protein Response and Endoplasmic Reticulum Stress after Mechanical Unloading in Dilated Cardiomyopathy. *Am J Physiol Heart Circ PhysiolHeart circulatory physiology* 309 (3), H459–H470. doi:10.1152/ajpheart.00056.2015

Choi, M. J., Park, E. J., Min, K. J., Park, J. W., and Kwon, T. K. (2011). Endoplasmic Reticulum Stress Mediates Withaferin A-Induced Apoptosis in Human Renal Carcinoma Cells. *Toxicol Vitro* 25 (3), 692–698. doi:10.1016/j.tiv.2011.01.010

Cissé, M., Duplan, E., and Checler, F. (2017). The Transcription Factor XBP1 in Memory and Cognition: Implications in Alzheimer's Disease. *Mol. Med.* 22, 905–917. doi:10.2119/molmed.2016.00229

Coe, H., and Michalak, M. (2009). Calcium Binding Chaperones of the Endoplasmic Reticulum. *Gen. Physiol. Biophys.* 28 Spec No Focus, F96–f103.

Cragg, G. M., and Newman, D. J. (2001). Natural Product Drug Discovery in the Next Millennium. *Pharm. Biol.* 39 Suppl 1 (Suppl. 1), 8–17. doi:10.1076/phbi.39.s1.8.0009

da Silva, D. C., Valentão, P., Andrade, P. B., and Pereira, D. M. (2020). Endoplasmic Reticulum Stress Signaling in Cancer and Neurodegenerative Disorders: Tools and Strategies to Understand its Complexity. *Pharmacol. Res.* 155, 104702. doi:10.1016/j.phrs.2020.104702

Dai, X., Kuang, Q., Sun, Y., Xu, M., Zhu, L., Ge, C., et al. (2022). Fisetin Represses Oxidative Stress and Mitochondrial Dysfunction in NAFLD through Suppressing GRP78-Mediated Endoplasmic Reticulum (ER) Stress. *J. Funct. Foods* 90, 104954. doi:10.1016/j.jff.2022.104954

Djoumbou Feunang, Y., Eisner, R., Knox, C., Chepelev, L., Hastings, J., Owen, G., et al. (2016). ClassyFire: Automated Chemical Classification with a Comprehensive, Computable Taxonomy. *J. Cheminform* 8, 61. doi:10.1186/s13321-016-0174-y

Doyle, K. M., Kennedy, D., Gorman, A. M., Gupta, S., Healy, S. J., and Samali, A. (2011). Unfolded Proteins and Endoplasmic Reticulum Stress in Neurodegenerative Disorders. *J. Cell. Mol. Med.* 15 (10), 2025–2039. doi:10.1111/j.1582-4934.2011.01374.x

Duran-Aniotz, C., Cornejo, V. H., Espinoza, S., Ardiles, Á. O., Medinas, D. B., Salazar, C., et al. (2017). IRE1 Signaling Exacerbates Alzheimer's Disease Pathogenesis. *Acta Neuropathol.* 134 (3), 489–506. doi:10.1007/s00401-017-1694-x

Ghemrawi, R., and Khair, M. (2020). Endoplasmic Reticulum Stress and Unfolded Protein Response in Neurodegenerative Diseases. *Int. J. Mol. Sci.* 21 (17), 6127. doi:10.3390/ijms21176127

Giordano, E., Davalos, A., Nicod, N., and Visioli, F. (2013). Hydroxytyrosol Attenuates Tunicamycin-Induced Endoplasmic Reticulum Stress in Human Hepatocarcinoma Cells. *Mol. Nutr. Food Res.* 58 (5), 954–962. doi:10.1002/mnfr.201300465

Gorbatyuk, M. S., and Gorbatyuk, O. S. (2013). The Molecular Chaperone GRP78/BiP as a Therapeutic Target for Neurodegenerative Disorders: a Mini Review. *J. Genet. Syndr. Gene Ther.* 4 (2), 128. doi:10.4172/2157-7412.1000128

Halliday, M., Radford, H., Sekine, Y., Moreno, J., Verity, N., Le Quesne, J., et al. (2015). Partial Restoration of Protein Synthesis Rates by the Small Molecule ISRIB Prevents Neurodegeneration without Pancreatic Toxicity. *Cell. Death Dis.* 6 (3), e1672. doi:10.1038/cddis.2015.49

Hamos, J. E., Oblas, B., Pulaski-Salo, D., Welch, W. J., Bole, D. G., and Drachman, D. A. (1991). Expression of Heat Shock Proteins in Alzheimer's Disease. *Neurology* 41 (3), 345–350. doi:10.1212/wnl.41.3.345

Hao, X., Yao, A., Gong, J., Zhu, W., Li, N., and Li, J. (2012). Berberine Ameliorates Pro-inflammatory Cytokine-Induced Endoplasmic Reticulum Stress in Human Intestinal Epithelial Cells *In Vitro*. *Inflammation* 35 (3), 841–849. doi:10.1007/s10753-011-9385-6

Hoozemans, J. J., Van Haastert, E. S., Nijholt, D. A., Rozemuller, A. J., Eikelenboom, P., and Scheper, W. (2009). The Unfolded Protein Response Is Activated in Pretangle Neurons in Alzheimer's Disease hippocampus. *Am. J. Pathol.* 174 (4), 1241–1251. doi:10.2353/ajpath.2009.080814

Hoozemans, J. J., Veerhuis, R., Van Haastert, E. S., Rozemuller, J. M., Baas, F., Eikelenboom, P., et al. (2005). The Unfolded Protein Response Is Activated in Alzheimer's Disease. *Acta Neuropathol.* 110 (2), 165–172. doi:10.1007/s00401-005-1038-0

Jayaseelan, K. V., Moreno, P., Truszkowski, A., Ertl, P., and Steinbeck, C. (2012). Natural Product-Likeness Score Revisited: an Open-Source, Open-Data Implementation. *BMC Bioinforma.* 13 (1), 106. doi:10.1186/1471-2105-13-106

Jia, S., Xu, X., Zhou, S., Chen, Y., Ding, G., and Cao, L. (2019). Fisetin Induces Autophagy in Pancreatic Cancer Cells via Endoplasmic Reticulum Stress- and Mitochondrial Stress-dependent Pathways. *Cell. Death Dis.* 10 (2), 142. doi:10.1038/s41419-019-1366-y

Jung, E. S., Hong, H., Kim, C., and Mook-Jung, I. (2015). Acute ER Stress Regulates Amyloid Precursor Protein Processing through Ubiquitin-dependent Degradation. *Sci. Rep.* 5 (1), 8805. doi:10.1038/srep08805

Kang, K. A., Piao, M. J., Madduma Hewage, S. R., Ryu, Y. S., Oh, M. C., Kwon, T. K., et al. (2016). Fisetin Induces Apoptosis and Endoplasmic Reticulum Stress in Human Non-small Cell Lung Cancer through Inhibition of the MAPK Signaling Pathway. *Tumour Biol.* 37 (7), 9615–9624. doi:10.1007/s13277-016-4864-x

Khan, S., Rammeloo, A. W., and Heikkila, J. J. (2012). Withaferin A Induces Proteasome Inhibition, Endoplasmic Reticulum Stress, the Heat Shock Response and Acquisition of Thermotolerance. *PLOS ONE* 7 (11), e50547. doi:10.1371/journal.pone.0050547

Kim, D. K., Kim, T. H., and Lee, S. J. (2016). Mechanisms of Aging-Related Proteinopathies in *Caenorhabditis elegans*. *Exp. Mol. Med.* 48 (10), e263. doi:10.1038/emm.2016.109

Kim, H., Park, B. S., Lee, K. G., Choi, C. Y., Jang, S. S., Kim, Y. H., et al. (2005). Effects of Naturally Occurring Compounds on Fibril Formation and Oxidative Stress of Beta-Amyloid. *J. Agric. Food Chem.* 53 (22), 8537–8541. doi:10.1021/jf051985c

Kraus, A., and Michalak, M. (2007). "Endoplasmic Reticulum Dynamics and Calcium Signaling," in *New Comprehensive Biochemistry*. Editors J. Krebs and M. Michalak (Amsterdam, Netherlands: Elsevier), 199–218. doi:10.1016/s0167-7306(06)41008-5

Lee, J. H., Won, S. M., Suh, J., Son, S. J., Moon, G. J., Park, U. J., et al. (2010). Induction of the Unfolded Protein Response and Cell Death Pathway in Alzheimer's Disease, but Not in Aged Tg2576 Mice. *Exp. Mol. Med.* 42 (5), 386–394. doi:10.3858/emm.2010.42.5.040

Liu, Y. Q., Jia, M. Q., Xie, Z. H., Liu, X. F., Hui-Yang, Y., Zheng, X. L., et al. (2017). Arrestins Contribute to Amyloid Beta-Induced Cell Death via Modulation of Autophagy and the α7nAch Receptor in SH-Sy5y Cells. *Sci. Rep.* 7 (1), 3446. doi:10.1038/s41598-017-01798-x

López-Antón, N., Rudy, A., Barth, N., Schmitz, M. L., Schmitz, L. M., Pettit, G. R., et al. (2006). The Marine Product Cephalostatin 1 Activates an Endoplasmic Reticulum Stress-specific and Apoptosome-independent Apoptotic Signaling Pathway. *J. Biol. Chem.* 281 (44), 33078–33086. doi:10.1074/jbc.M607904200

McInnes, L. H, J. (2018). *UMAP: Uniform Manifold Approximation and Projection for Dimension Reduction*. ArXiv e-prints 1802.03426.

Meglen, R. R. (1992). Examining Large Databases: a Chemometric Approach Using Principal Component Analysis. *Mar. Chem.* 39 (1), 217–237. doi:10.1016/0304-4203(92)90103-H

Moreno, J. A., Halliday, M., Molloy, C., Radford, H., Verity, N., Axten, J. M., et al. (2013). Oral Treatment Targeting the Unfolded Protein Response Prevents Neurodegeneration and Clinical Disease in Prion-Infected Mice. *Sci. Transl. Med.* 5, 206ra138. doi:10.1126/scitranslmed.3006767)

Navarrete, C., Sancho, R., Caballero, F. J., Pollastro, F., Fiebich, B. L., Sterner, O., et al. (2006). Basiliolides, a Class of Tetracyclic C19 Dilactones from Thapsia Garganica, Release Ca(2+) from the Endoplasmic Reticulum and Regulate the Activity of the Transcription Factors Nuclear Factor of Activated T Cells, Nuclear Factor-kappaB, and Activator Protein 1 in T Lymphocytes. *J. Pharmacol. Exp. Ther.* 319 (1), 422–430. doi:10.1124/jpet.106.108209

Nonaka, T., Watanabe, S. T., Iwatsubo, T., and Hasegawa, M. (2010). Seeded Aggregation and Toxicity of {alpha}-Synuclein and Tau: Cellular Models of Neurodegenerative Diseases. *J. Biol. Chem.* 285 (45), 34885–34898. doi:10.1074/jbc.M110.148460

O'connor, T., Sadleir, K. R., Maus, E., Velliquette, R. A., Zhao, J., Cole, S. L., et al. (2008). Phosphorylation of the Translation Initiation Factor eIF2alpha Increases BACE1 Levels and Promotes Amyloidogenesis. *Neuron* 60 (6), 988–1009. doi:10.1016/j.neuron.2008.10.047

Ogen-Shtern, N., Ben David, T., and Lederkremer, G. Z. (2016). Protein Aggregation and ER Stress. *Brain Res.* 1648, 658–666. doi:10.1016/j.brainres.2016.03.044

Pedregosa, F., Varoquaux, G., Gramfort, A., Michel, V., Thirion, B., Grisel, O., et al. (2011). Scikit-learn: Machine Learning in Python. *J. Mach. Learn. Res.* 12, 2825–2830.

Pereira, D. M., Valentão, P., Correia-Da-Silva, G., Teixeira, N., and Andrade, P. B. (2015). Translating Endoplasmic Reticulum Biology into the Clinic: a Role for ER-Targeted Natural Products? *Nat. Prod. Rep.* 32 (5), 705–722. doi:10.1039/C4NP00102H

Pimentel, A. A., Felibertt, P., Sojo, F., Colman, L., Mayora, A., Silva, M. L., et al. (2012). The Marine Sponge Toxin Agelasine B Increases the Intracellular Ca(2+) Concentration and Induces Apoptosis in Human Breast Cancer Cells (MCF-7). *Cancer Chemother. Pharmacol.* 69 (1), 71–83. doi:10.1007/s00280-011-1677-x

Plate, L., Cooley, C. B., Chen, J. J., Paxman, R. J., Gallagher, C. M., Madoux, F., et al. (2016). Small Molecule Proteostasis Regulators that Reprogram the ER to Reduce Extracellular Protein Aggregation. *eLife* 5, e15550. doi:10.7554/eLife.15550

Radford, H., Moreno, J. A., Verity, N., Halliday, M., and Mallucci, G. R. (2015). PERK Inhibition Prevents Tau-Mediated Neurodegeneration in a Mouse Model of Frontotemporal Dementia. *Acta Neuropathol.* 130 (5), 633–642. doi:10.1007/s00401-015-1487-z

Rcom-H'cheo-Gauthier, A. N., Meedeniya, A. C., and Pountney, D. L. (2017). Calcipotriol Inhibits α-synuclein Aggregation in SH-Sy5y Neuroblastoma Cells by a Calbindin-d28k-dependent Mechanism. *J. Neurochem.* 141 (2), 263–274. doi:10.1111/jnc.13971

Roussel, B. D., Kruppa, A. J., Miranda, E., Crowther, D. C., Lomas, D. A., and Marciniak, S. J. (2013). Endoplasmic Reticulum Dysfunction in Neurological Disease. *Lancet Neurol.* 12 (1), 105–118. doi:10.1016/s1474-4422(12)70238-7

Sang, J. C., Hidari, E., Meisl, G., Ranasinghe, R. T., Spillantini, M. G., and Klenerman, D. (2021). Super-resolution Imaging Reveals α-synuclein Seeded Aggregation in SH-Sy5y Cells. *Commun. Biol.* 4 (1), 613. doi:10.1038/s42003-021-02126-w

Santos, L. E., and Ferreira, S. T. (2018). Crosstalk between Endoplasmic Reticulum Stress and Brain Inflammation in Alzheimer's Disease. *Neuropharmacology* 136, 350–360. doi:10.1016/j.neuropharm.2017.11.016

Sharma, R., Srivastava, T., Pandey, A. R., Mishra, T., Gupta, B., Reddy, S. S., et al. (2021). Identification of Natural Products as Potential Pharmacological Chaperones for Protein Misfolding Diseases. *ChemMedChem* 16 (13), 2146–2156. doi:10.1002/cmdc.202100147

Shen, B. (2015). A New Golden Age of Natural Products Drug Discovery. *Cell.* 163 (6), 1297–1300. doi:10.1016/j.cell.2015.11.031

Shih, Y. L., Hung, F. M., Lee, C. H., Yeh, M. Y., Lee, M. H., Lu, H. F., et al. (2017). Fisetin Induces Apoptosis of HSC3 Human Oral Cancer Cells through Endoplasmic Reticulum Stress and Dysfunction of Mitochondria-Mediated Signaling Pathways. *Vivo* 31 (6), 1103–1114. doi:10.21873/invivo.11176

Shinde, V., Kotla, P., Strang, C., and Gorbatyuk, M. (2016). Unfolded Protein Response-Induced Dysregulation of Calcium Homeostasis Promotes Retinal Degeneration in Rat Models of Autosomal Dominant Retinitis Pigmentosa. *Cell. Death Dis.* 7 (2), e2085. doi:10.1038/cddis.2015.325

Sorokina, M., Merseburger, P., Rajan, K., Yirik, M. A., and Steinbeck, C. (2021). COCONUT Online: Collection of Open Natural Products Database. *J. Cheminform* 13 (1), 2. doi:10.1186/s13321-020-00478-9

Syed, D. N., Lall, R. K., Chamcheu, J. C., Haidar, O., and Mukhtar, H. (2014). Involvement of ER Stress and Activation of Apoptotic Pathways in Fisetin Induced Cytotoxicity in Human Melanoma. *Arch. Biochem. Biophys.* 563, 108–117. doi:10.1016/j.abb.2014.06.034

Taalab, Y. M., Ibrahim, N., Maher, A., Hassan, M., Mohamed, W., Moustafa, A. A., et al. (2018). Mechanisms of Disordered Neurodegenerative Function: Concepts and Facts about the Different Roles of the Protein Kinase RNA-like Endoplasmic Reticulum Kinase (PERK). *Rev. Neurosci.* 29 (4), 387–415. doi:10.1515/revneuro-2017-0071

Tahtamouni, L. H., Nawasreh, M. M., Al-Mazaydeh, Z. A., Al-Khateeb, R. A., Abdellatif, R. N., Bawadi, R. M., et al. (2018). Cephalostatin 1 Analogues Activate Apoptosis via the Endoplasmic Reticulum Stress Signaling Pathway. *Eur. J. Pharmacol.* 818, 400–409. doi:10.1016/j.ejphar.2017.11.025

Verma, A., Bhatt, A. N., Farooque, A., Khanna, S., Singh, S., and Dwarakanath, B. S. (2011). Calcium Ionophore A23187 Reveals Calcium Related Cellular Stress as "I-Bodies": an Old Actor in a New Role. *Cell. Calcium* 50 (6), 510–522. doi:10.1016/j.ceca.2011.08.007

Wang, Z. S., Lu, F. E., Xu, L. J., and Dong, H. (2010). Berberine Reduces Endoplasmic Reticulum Stress and Improves Insulin Signal Transduction in Hep G2 Cells. *Acta Pharmacol. Sin.* 31 (5), 578–584. doi:10.1038/aps.2010.30

Weidner, J., Jarenbäck, L., Åberg, I., Westergren-Thorsson, G., Ankerst, J., Bjermer, L., et al. (2018). Endoplasmic Reticulum, Golgi, and Lysosomes Are Disorganized in Lung Fibroblasts from Chronic Obstructive Pulmonary Disease Patients. *Physiol. Rep.* 6 (5), e13584. doi:10.14814/phy2.13584

Xiang, C., Wang, Y., Zhang, H., and Han, F. (2017). The Role of Endoplasmic Reticulum Stress in Neurodegenerative Disease. *Apoptosis* 22 (1), 1–26. doi:10.1007/s10495-016-1296-4

Xicoy, H., Wieringa, B., and Martens, G. J. (2017). The SH-Sy5y Cell Line in Parkinson's Disease Research: a Systematic Review. *Mol. Neurodegener.* 12 (1), 10. doi:10.1186/s13024-017-0149-0

Zhang, Z., Li, B., Meng, X., Yao, S., Jin, L., Yang, J., et al. (2016). Berberine Prevents Progression from Hepatic Steatosis to Steatohepatitis and Fibrosis by Reducing Endoplasmic Reticulum Stress. *Sci. Rep.* 6, 20848. doi:10.1038/srep20848

Zhou, W., Chang, L., Fang, Y., Du, Z., Li, Y., Song, Y., et al. (2016). Cerebral Dopamine Neurotrophic Factor Alleviates Aβ25-35-Induced Endoplasmic Reticulum Stress and Early Synaptotoxicity in Rat Hippocampal Cells. *Neurosci. Lett.* 633, 40–46. doi:10.1016/j.neulet.2016.09.008

Conflict of Interest: The authors declare that the research was conducted in the absence of any commercial or financial relationships that could be construed as a potential conflict of interest.

The reviewer JR declared a past co-authorship with the author DMP to the handling editor.

Publisher's Note: All claims expressed in this article are solely those of the authors and do not necessarily represent those of their affiliated organizations, or those of the publisher, the editors and the reviewers. Any product that may be evaluated in this article, or claim that may be made by its manufacturer, is not guaranteed or endorsed by the publisher.